Published in final edited form as:
Science. 2009 August 7; 325(5941): 725–730. doi:10.1126/science.1174251.

Folding DNA into Twisted and Curved Nanoscale Shapes

Hendrik Dietz[1,2,*], **Shawn M. Douglas**[1,2,3], and **William M. Shih**[1,2,3,†]
[1]Department of Cancer Biology, Dana-Farber Cancer Institute, Boston, MA 02115

[2]Department of Biological Chemistry and Molecular Pharmacology, Harvard Medical School, Boston, MA 02115

[3]Wyss Institute for Biologically Inspired Engineering, Harvard University, Cambridge, MA 02138

Abstract

We demonstrate the ability to engineer complex shapes that twist and curve at the nanoscale from DNA. Through programmable self-assembly, strands of DNA are directed to form a custom-shaped bundle of tightly crosslinked double helices, arrayed in parallel to their helical axes. Targeted insertions and deletions of base pairs cause the DNA bundles to develop twist of either handedness or to curve. The degree of curvature could be quantitatively controlled, and a radius of curvature as tight as 6 nanometers was achieved. We also combined multiple curved elements to build several different types of intricate nanostructures, such as a wireframe beach ball or square-toothed gears.

The sequences of DNA molecules can be engineered so that complex higher-order structures form as multiple double-helical segments connected through numerous turn regions. Programmable self-assembly based on DNA directed to branch in this way offers an attractive route to creating particular shapes on the 1 to 100 nm scale [1–4], as evidenced by its use in constructing two-dimensional (2D) crystals [5], nanotubes [6–11], and three-dimensional (3D) wireframe polyhedra [12–17]. More recently, oligonucleotide-'staple-strand'-assisted folding of a multiple-kilobase 'scaffold strand' has been introduced as a powerful method to direct the self-assembly of custom-shaped, mega-dalton-scale, planar arrays of anti-parallel helices connected through turn regions [18]. In this 'scaffolded-DNA-origami' method, each staple strand base-pairs along part of its length with a complementary segment of the scaffold strand, and then abruptly switches to base-pair with another complementary scaffold segment that may be quite distant in the scaffold primary sequence. A single staple strand may pair with several scaffold-strand segments in accordance with this switching strategy. Association with hundreds of such staple strands constrains the scaffold strand to helical paths that raster back and forth into a target anti-parallel-array arrangement.

We recently extended DNA-origami to 3D nanoconstruction with a design strategy that can be conceptualized as stacking corrugated sheets of antiparallel helices [19]. The resulting structures resemble bundles of double helices constrained to a honeycomb lattice (an example is shown in Fig. 1A; also see Figs. S7–S24 for detailed examples of how staple strands can be programmed to link the scaffold strand into an anti-parallel array of honeycomb-pleated helices). The number, arrangement, and individual lengths of helices can be tuned to produce a variety of 3D shapes; we have developed a graphical software tool to aid in the design process

†To whom correspondence should be addressed. William_Shih@dfci.harvard.edu.
*Present address: Physik Department, Technische Universität München, Garching b. München, D-85748 Germany

One-sentence summary
Site-directed insertions and deletions of base pairs direct twist and curvature in bundled DNA arrays.

[20]. Here we expand the design space of accessible DNA-origami shapes to include a rich diversity of nanostructures with designed twist and curvature.

In our honeycomb-array framework, every double helix has up to three nearest neighbors (Fig. 1A) and is designed to connect to each by anti-parallel strand crossovers, which are covalent phosphate linkages in the same form as found in naturally occurring Holliday junctions. For explanatory purposes, here we assume that only staple strands, and not the scaffold strand, can cross over to form a Holliday junction between adjacent double helices [19]. Every 7 base pairs (bp), the helical path of a strand rotates by 240°, assuming a B-form-DNA twist density of 10.5 bp/turn. Therefore, 14 bp gives rise to a rotation of 120° plus 360°, and 21 bp gives rise to a rotation of 0° plus 2 times 360°. As a result, anti-parallel strand crossovers to one of the three nearest neighbors at 0°, 120°, and 240° can be engineered to occur once every 7 bp. Thus, along the helical axis of the whole honeycomb array, crossovers only can occur at positions that coincide with conceptual planes perpendicular to that axis spaced at 7 bp intervals.

These crossover planes can be used as a reference to conceive the honeycomb-pleated helix bundle as a three-dimensional array of cells that by default each contain a 7 bp-long double-helical DNA fragment (Fig. 1B) that is mechanically coupled to its nearest neighbors. This abstraction of the DNA bundle as a collection of array cells is key for understanding how site-directed insertions and deletions of base pairs in the bundle can control twist and curvature.

We systematically adjusted the number of base pairs in selected subsets of array cells to realize DNA shapes that globally twist or bend along their helix-parallel axes. Because any array-cell DNA fragment is physically constrained by its neighbors in the honeycomb array, deletion of a base pair results in a local overwinding and tensile strain for that fragment, which causes it to exert a left-handed torque and a pull on its neighbors (Fig. 1C, top). The overwind strain can be relieved by a compensatory global left-handed twist of the bundle along its helix-parallel axis, while the tensile strain can be relieved by a compensatory global bend of the bundle towards that fragment along its helix-parallel axis. In the same way, insertion of a base pair into an array cell results in a local underwinding and compressive strain (Fig. 1C, bottom) that can be relieved by a compensatory global right-handed twist and bend away from the fragment along the helix-parallel axis.

Destructive cancellation of compensatory global bend deformations and constructive reinforcement of compensatory global twist deformations can be implemented, for example, by distribution of only deletions or of only insertions in the bundle as depicted for Fig. 1D. The bundle with only deletions is analogous to the architecture of protein coiled coils, where overwinding of right-handed alpha helices from 3.6 to 3.5 amino acids per turn, enforced by heptad-repeat phasing, is compensated by a global left-handed twist. Conversely, destructive cancellation of global twist deformations and constructive reinforcement of global bend deformations can be implemented, for example, by distribution of a gradient of deletions to insertions of base pairs through a bundle's cross section as depicted in Fig. 1E. Steeper gradients of deletions to insertions can be implemented to achieve greater degrees of curvature.

In order to assess whether global twisting can be implemented, we chose as a model system a ten row, six-helix-per-row (10 by 6) bundle comprised of 60 tightly interconnected DNA double helices (Fig. 2) that we previously had identified as a well-behaved folding architecture [19,20] and whose ribbon-like (as opposed to tube-like) structure makes observation of twisting more facile. We designed three versions of this bundle. In the default version that is designed not to twist, 19 crossover planes are spaced evenly in 7 bp steps across a length of 126 bp, or 12 complete turns at 10.5 bp/turn. We designed a second version of the 10 by 6 bundle in which we deleted a single base pair from every third array cell along each helix. Thus, one-third of all array cells contain overtwisted DNA fragments, resulting in a bundle with a length of 120

bp and an average twist density of 10 bp/turn. We designed a third version of the 10 by 6 bundle in which we added a single base pair to every third array cell, resulting in a shape with a length of 132 bp and an average twist density of 11 bp/turn (see Figs. S7 to S9 for design details).

The 10 by 6 bundles were folded by a two-step process. The first step involved initialization of the system by incubation at 80°C of the appropriate mixture of scaffold and staple strands in buffered solution. The second step involved gradual cooling of the strand suspension to room temperature. Next, the sample was subjected to agarose-gel electrophoresis. The fastest migrating band (excluding the free staple strands) typically represented monomeric species. Thus excision of this band from the gel, followed by recovery of the embedded particles by centrifugation through a cellulose-acetate filter, resulted in enrichment of well-folded particles. These gel-purified particles then were imaged by negative-stain transmission electron microscopy (TEM) (see Note S1 for imaging methods and Fig. S3 for additional zoom-out images). As previously reported, no systematic deformations were found in the default 10.5 bp/turn version of the bundle (Fig. 2A, bottom left) [19]. However, particles designed with locally overtwisted DNA (Fig. 2B, bottom left) or locally undertwisted DNA (Fig. 2C, bottom left) appear to exhibit a global twist deformation when oriented such that they are viewed down the helical-axis interface or down the six-helix-wide side. The deformed appearance is not obvious for particles that are oriented with the 10-helix-wide side oriented parallel to the grid surface. Surprisingly, the 11 bp/turn designed twist density improved overall folding quality (Fig. 2F) of the 10 by 6 bundle. We speculate that the increased spacing between crossover planes may allow greater electrostatic-repulsion-driven bowing out of helices, that therefore is easier to achieve. An alternative speculative explanation derives from the observation that, for helices surrounded by three neighbors in the honeycomb array, crossovers occur every 7 bp. An increased spacing of 8 bp may improve stability of these segments in a manner that affects the rate-limiting steps for folding. Systematic experiments in the future will be required for elucidating the determinants of folding speed and quality.

To verify the apparent twist, we separately polymerized each of the 10 by 6 bundle versions along the helical axes to form ribbons. When comprised of bundles designed with only default 7 bp array cells, the resulting ribbons appeared completely straight with no detectable global twist (Fig. 2A, top-right). In contrast, for both the versions with locally overtwisted and with locally undertwisted DNA fragments, we consistently observed ribbons that clearly twist (see Fig. S3 for additional zoom-out image data). In order to determine the chirality of these twisted ribbons, we collected tilt-pair images by rotating the TEM goniometer (Fig. 2, D and E). For ribbons polymerized from bundles with locally undertwisted DNA, we observed that the nodes consistently moved upward upon an 80° counterclockwise sample-plane rotation. The experimental geometry (Fig 2D, bottom) provides an unequivocal identification of the global twist as right-handed. Conversely, for ribbons constructed from bundles with locally overtwisted DNA, we observed that the ribbon nodes consistently moved downward upon the same sample rotation, thus revealing a global left-handed twist.

We quantified the twist frequency by measuring the distance between consecutive nodes for multiple ribbons (Fig. 2G) and then plotting global twist per turn as observed for each version of the 10 by 6 bundles versus initially imposed double-helical twist density (Fig. 2H). Different architectures likely will exhibit global twisting that will vary in absolute magnitude but not in sign from the values observed for the 10 by 6 bundle because of differences in resistance to torsion as a function of cross-sectional shape. For example, a 60-helix bundle with a more extended cross-section (e.g. 30 by 2 helices) would be expected to exhibit more global twist at the same initially imposed local double-helical twist density due to the lower torsional stiffness. We also experimentally observed global twist for a 3 by 6 bundle architecture, but due to the square-like cross section, it was difficult to determine the location of the nodes and thereby quantify the magnitude of twisting.

These results imply that average double-helical twist density must be carefully considered during DNA-nanostructure design to avoid unwanted global twist deformations. Global twisting has been observed for DNA nanotubes assembled from oligonucleotide-based tiles with double-helical twist densities deviating from 10.5 bp/turn [21,22]. Planar DNA origami [18] have been designed with an average twist density of 10.67 bp/turn. Intrinsic global twist of such designs as exists in solution, however, might not be obvious from image analysis of particles flattened by adhesion to surfaces.

We next explored the use of balanced gradients of insertions and deletions to produce global bend with no global twist by constructing seven versions of a three row, six-helix-per-row (3 by 6) bundle (Fig. 3A). The design contains 61 crossover planes evenly spaced along the helical axis. Between 15 crossover planes in the middle of the bundle, we implemented gradients of insertions and deletions across the short axis of the cross section (red segment in the models in Fig. 3 A–G, see Figs. S10 to S18 for design details). We implemented increasingly steep gradients (Fig. 3H, insets and Figs. S10 to S18) up to extreme deviations from native B-form DNA twist density, where one side of the 3 by 6 bundle has an average twist density of only 6 bp/turn while the opposite side has a twist density of as high as 15 bp/turn. We used a toy model that considers DNA as a continuum rod with elastic bending, stretch-compression, and twist-stretch coupling (see Note S2 and Fig. S1) and an iterative refinement procedure to identify gradients that produce bend angles from 30° to 180° in 30° steps with radii of curvature ranging from 64 nm down to 6 nm.

Folding of five of the seven 3 by 6 bundle versions resulted in products that migrate as sharp bands on a 2% agarose gel (Fig. 3H), indicating folding into an overall homogeneous shape, while the 150° and 180° versions migrate as more ‘fuzzy’ bands, which suggests that a greater degree of shape heterogeneity is present. The latter two versions coincide with the two steepest insertion/deletion gradients. Such stark deviations from B-form DNA twist density apparently compromise folding quality and increase the frequency of defective particles. We also note that the gel mobility decreases with increasing gradient of insertions and deletions, indicating pronounced changes in the aspect ratio of the particles.

We used negative-stain TEM to study the appearance of the particles (Fig. 3A–G). The particles mainly adsorbed in two orientations on the TEM grids and exhibited a ‘smooth’ appearance when oriented with the long axis of the bundle cross section parallel to the grid, but exhibited three pronounced stripes when oriented with the short axis parallel to the TEM grid (see Note S4 and Fig. S2 for a more detailed explanation of the origin of the stripes as well as Fig. S4 for image data with multiple particle orientations). The orientation giving rise to the ‘stripy’ appearance allows for a direct assessment of the extent of the induced bending.

Bend angles ranging from 30° to 180° as well as sharply bent radii of curvature down to 6 nm, close to the extreme bending of DNA found in the nucleosome [23], could be realized. Figs. 3I and 3J give a sense of the shape homogeneity exemplified by two bundle versions designed to bend at 30° and 150°, respectively. Additional zoom-out image data for each version of the 3 by 6 helix bundles is provided in Fig. S4.

We quantified the distribution of bend angles for each version in the series of bundles. To avoid bias from obviously defective particles, we analyzed only those where three pronounced stripes were clearly discernible along the entire length. As an example, particles marked with an asterisk in Figs. 3I and 3J do not satisfy that criterion. We observed the fraction of particles that failed this criterion was about 50% for radii of curvature above 10 nm but increased as a function of tightness of radii of curvature above 10 nm (Fig. S4). Histograms of bend angles observed for the seven different 3 by 6 bundle versions are displayed in Fig. 3K. The distributions each have a half-width at half maximum of 5° to 9°. Our toy model predicts

thermally induced angular fluctuations with a standard deviation from the mean bend angle of about 2.5° (see Note S2 and Fig. S1). The discrepancy between expected and observed distribution widths may be due to defects. Defective helices confer bending 'individuality' to each particle, because defects change the effective gradient of insertions and deletions as well as the compliance of a defective helix in the bundle. A future challenge will be to improve folding quality such that thermal fluctuations alone determine the angular precision of any produced shape. Our toy model can identify insertion and deletion patterns to an accuracy of 3° for desired mean bend angles less than or equal to 120°, although changes in environmental conditions may require adjustment of model parameters. We expect our method for generating DNA shapes with tunable bending to be generally applicable for a wide range of bundle cross-section architectures, as long as extreme deviations from canonical B-form DNA twist density (<6 bp/turn or >15 bp/turn) are avoided.

To illustrate the diversity of curved shapes now accessible, we designed a DNA bundle bearing three 'teeth' that is programmed to fold into a half circle with a 25 nm radius (Fig. 4A, also see Fig. S19 for design details, and Fig. S5 for additional zoom-out image data). Using hierarchical assembly, two of these bundles can be combined into a circular object that resembles a nanoscale gear with six teeth. The teeth exhibited a greater frequency of folding defects than the body, at a rate of about one defective tooth out of three, perhaps related to their small size (only 42 bp long per double helix). About one third of multimeric complexes were observed to be the target cyclic dimers, versus noncyclic dimers and higher order multimers. By adjusting the gradient of insertions and deletions, the bundle can be tuned to fold into a quarter circle with a 50 nm radius (Fig. 4B, see also Fig. S20 for design details). By connecting four of these quarter circles, a gear with 12 teeth can be manufactured. In this case, only about a tenth of the multimeric complexes were observed to be the target cyclic tetramers. In the future, target cyclization may be improved for objects designed with taller interfaces that resist out-of-plane bending and that are more tolerant of folding defects.

Three-dimensional spherical shapes can be created as well (Fig. 4C). We designed a 50-nm-wide spherical wireframe object that resembles a beach ball by programming six interconnected vertices, each composed of two crossed six-helix bundles, to bend such that a projection of the edges of an octahedron onto a circumscribing sphere is completed (see Fig. S21 for design details). We further designed a concave and a convex triangle (Figs. 4D, 4E, and Fig. S22 and S23 for design details), and a spiral consisting of six segments of a six-helix bundle that each are programmed to bend into a half circle with increasing radii of curvature (Fig. 4F, see Fig. S24 for design details). The convex triangle is designed as a hierarchically assembling homotrimer. For this design, about one-third of multimeric complexes were observed to be the target cyclic trimers (additional image data on all objects shown in Fig. 4 is provided in Fig. S6).

Precisely arranged bent DNA and associated DNA-binding proteins play an important role in transcriptional regulation and genomic packaging [24–26]. Programmable DNA bending might prove useful as a probe to study the propensity of such proteins to bind pre-bent DNA substrates, and also to probe the propensity of different DNA sequences to adopt specifically bent conformations [27].

Supplementary Material

Refer to Web version on PubMed Central for supplementary material.

References And Notes

1. Seeman NC. DNA in a material world. Nature 2003;421(6921):427–431. [PubMed: 12540916]

2. Seeman NC. Nucleic acid junctions and lattices. J Theor Biol 1982;99(2):237–247. [PubMed: 6188926]
3. Fu TJ, Seeman NC. DNA double-crossover molecules. Biochemistry 1993;32(13):3211–3220. [PubMed: 8461289]
4. Li XJ, et al. Antiparallel DNA double crossover molecules as components for nanoconstruction. J. Am. Chem. Soc 1996;118:6131–6140.
5. Winfree E, et al. Design and self-assembly of two-dimensional DNA crystals. Nature 1998 Aug 6;394 (6693):539–544. [PubMed: 9707114]
6. Yan H, et al. DNA-templated self-assembly of protein arrays and highly conductive nanowires. Science 2003;301(5641):1882–1884. [PubMed: 14512621]
7. Rothemund PW, et al. Design and characterization of programmable DNA nanotubes. J. Am. Chem. Soc 2004;126:16344–16352. [PubMed: 15600335]
8. Mathieu F, et al. Six-helix bundles designed from DNA. Nano Lett 2005;5:661–665. [PubMed: 15826105]
9. Douglas SM, Chou JJ, Shih WM. DNA-nanotube-induced alignment of membrane proteins for NMR structure determination. Proc Natl Acad Sci U S A 2007 Apr 17;104(16):6644–6648. [PubMed: 17404217]
10. Liu D, et al. DNA nanotubes self-assembled from triple-crossover tiles as templates for conductive nanowires. Proc Natl Acad Sci U S A 2004;101(3):717–722. [PubMed: 14709674]
11. Yin P, et al. Programming DNA tube circumferences. Science 2008;321(5890):824–826. [PubMed: 18687961]
12. Goodman RP, et al. Rapid chiral assembly of rigid DNA building blocks for molecular nanofabrication. Science 2005;310:1661–1665. [PubMed: 16339440]
13. Chen JH, Seeman NC. Synthesis from DNA of a molecule with the connectivity of a cube. Nature 1991 Apr 18;350(6319):631–633. [PubMed: 2017259]
14. Zhang Y, Seeman NC. The construction of a DNA truncated octahedron. J. Am. Chem. Soc 1994;116:1661–1669.
15. He Y, et al. Hierarchical self-assembly of DNA into symmetric supramolecular polyhedra. Nature 2008 Mar 13;452(7184):198–201. [PubMed: 18337818]
16. Zhang C, et al. Conformational flexibility facilitates self-assembly of complex DNA nanostructures. Proc Natl Acad Sci U S A 2008;105(31):10665–10669. [PubMed: 18667705]
17. Shih WM, Quispe JD, Joyce GF. A 1.7-kilobase single-stranded DNA that folds into a nanoscale octahedron. Nature 2004;427(6975):618–621. [PubMed: 14961116]
18. Rothemund PW. Folding DNA to create nanoscale shapes and patterns. Nature 2006;440(7082):297–302. [PubMed: 16541064]
19. Douglas SM, et al. Self-assembly of DNA into nanoscale three dimensional shapes. Nature 2009;459 (7245):414–418. [PubMed: 19458720]
20. Douglas SM, et al. Rapid prototyping of three-dimensional DNA-origami shapes with caDNAno. Nucleic Acids Research. 2009 Jun 16;Epub ahead of print
21. Grason GM, Bruinsma RF. Chirality and equilibrium biopolymer bundles. Phys Rev Lett 2007;99 (9):098101. [PubMed: 17931038]
21. Mitchell JC, et al. Self-assembly of chiral DNA nanotubes. J Am Chem Soc 2004;126(50):16342–16343. [PubMed: 15600334]
22. Lin C, et al. Mirror image DNA nanostructures for chiral supramolecular assemblies. Nano Lett 2009;9(1):433–436. [PubMed: 19063615]
23. Luger K, et al. Crystal structure of the nucleosome core particle at 2.8 A resolution. Nature 1997;389 (6648):251–260. [PubMed: 9305837]
24. Borowiec JA, et al. DNA supercoiling promotes formation of a bent repression loop in lac DNA. J Mol Biol 1987;196(1):101–111. [PubMed: 3656441]
25. Chang J, et al. Cryo-EM asymmetric reconstruction of bacteriophage P22 reveals organization of its DNA packaging and infecting machinery. Structure 2006;14(6):1073–1082. [PubMed: 16730179]
26. Garcia HG, et al. Biological consequences of tightly bent DNA: the other life of a macromolecular celebrity. Biopolymers 2007;85:115–130. [PubMed: 17103419]

27. Parker SC, et al. Local DNA Topography Correlates with Functional Noncoding Regions of the Human Genome. Science. 2009

28. HD thanks Andres E. Leschziner for training in electron microscopy and generous supply of image processing hardware and software. This work was supported by Claudia Adams Barr Program Investigator, Wyss Institute for Biologically Inspired Engineering, and NIH New Innovator (1DP2OD004641-01) grants to WMS and Feodor-Lynen Humboldt Fellowship to HD.

29. HD, SMD, and WMS designed research. HD developed rules for twisting and bending. HD and SMD designed all shapes. HD and SMD collected data, HD analyzed data. SMD provided caDNAno software support. HD, WMS, and SMD wrote the manuscript.

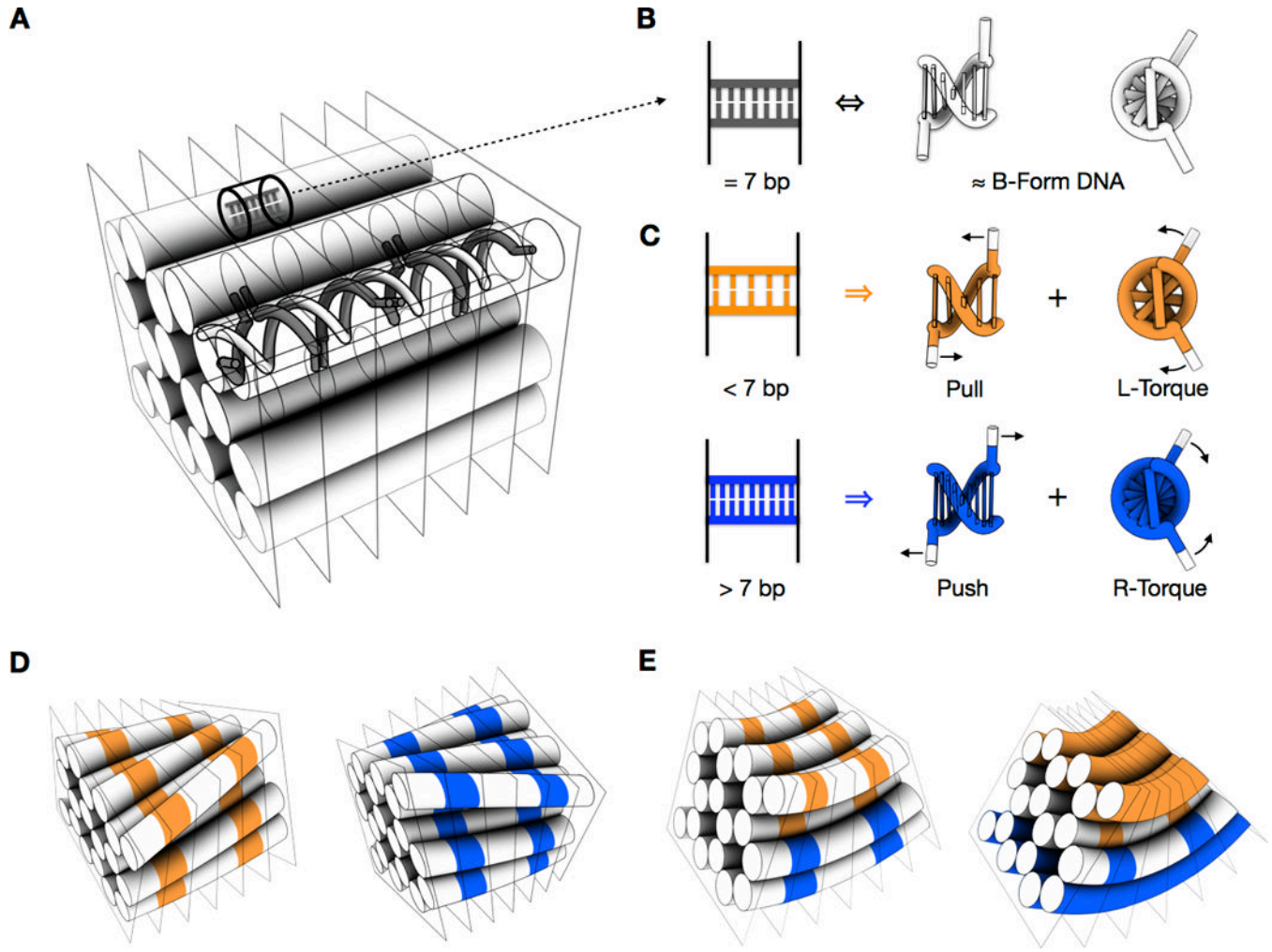

Figure 1.

Design principles for controlling twist and curvature in DNA bundles. **(A)** Double helices are constrained to a honeycomb arrangement by staple-strand crossovers. Semi-transparent crossover planes mark the locations of strand crossovers between neighboring helices, which are spaced at 7 bp intervals along the helical axis. From left to right, each plane contains a class of crossovers rotated in-plane by 240° clockwise with respect to the preceding plane. The crossover planes divide the bundle conceptually into helix fragments that can be viewed as residing in array cells (one cell is highlighted). **(B)** Array cell with default content of 7 bp, which exerts no stress on its neighbors. **(C)** Above, array cell with content of 5 bp, which is under strain and therefore exerts a left-handed torque and a pull on its neighbors. Below, array cell with content of 9 bp, which is under strain and therefore exerts a right-handed torque and a push on its neighbors. Force vectors are shown on only two of the four strand ends of the array-cell fragment for clarity. **(D)** Left (right), site-directed deletions (insertions) installed in selected array cells indicated in orange (blue) result in global left-handed (right-handed) twisting with cancellation of compensatory global bend contributions. **(E)** Site-directed base-pair deletions, indicated in orange, and base-pair insertions, indicated in blue, can be combined to induce tunable global bending of the DNA bundle with cancellation of compensatory global twist contributions.

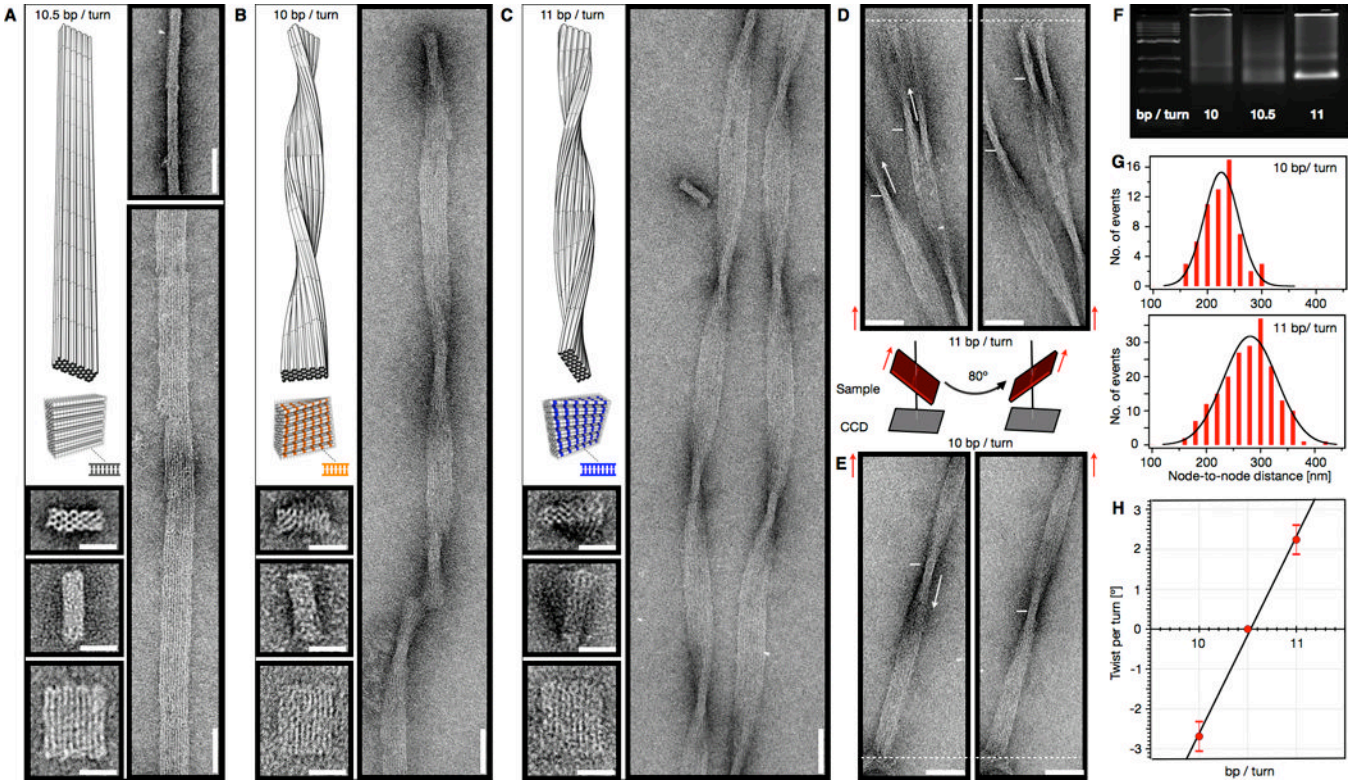

Figure 2.

Deviations from 10.5 bp/turn twist density induce global twisting. **(A–C)** Top left: models of a 10 by 6-helix DNA bundle (red) with 10.5, 10, and 11 bp/turn average double-helical twist density, respectively, and models of ribbons when polymerized (silver). Bottom left: monomeric particles as observed by negative-stain transmission electron microscopy. Scale bars: 20 nm. Right: polymeric ribbons as observed by TEM. Scale bars: 50 nm. **(D, E)** Tilt-pair images of twisted ribbons polymerized from 11 bp/turn (D) and 10 bp/turn (E) 10 by 6-helix bundles, recorded at goniometer angles 40° and −40°. Arrows indicate the observed upward (for 11 bp/turn) or downward (for 10 bp/turn) direction of movement of the twisted-ribbon nodes. Dashed line provides reference point (ends of ribbons remain stationary upon goniometer rotation). **(F)** Ethidium-bromide-stained 2% agarose gel, comparing migration of unpurified folded bundles. **(G)** Histograms of the observed node-to-node distance in twisted ribbons as observed in negative-stain TEM micrographs. Left-handed and right-handed ribbons undergo half-turns every 235±(32 s.d.) nm (N=62) and 286±(48 s.d.) nm (N=197), respectively. **(H)** Plot of observed global compensatory twist per turn versus double-helical twist density initially imposed by design. A value of 0.335 nm/bp was used to calculate global twist per turn from values obtained in (G).

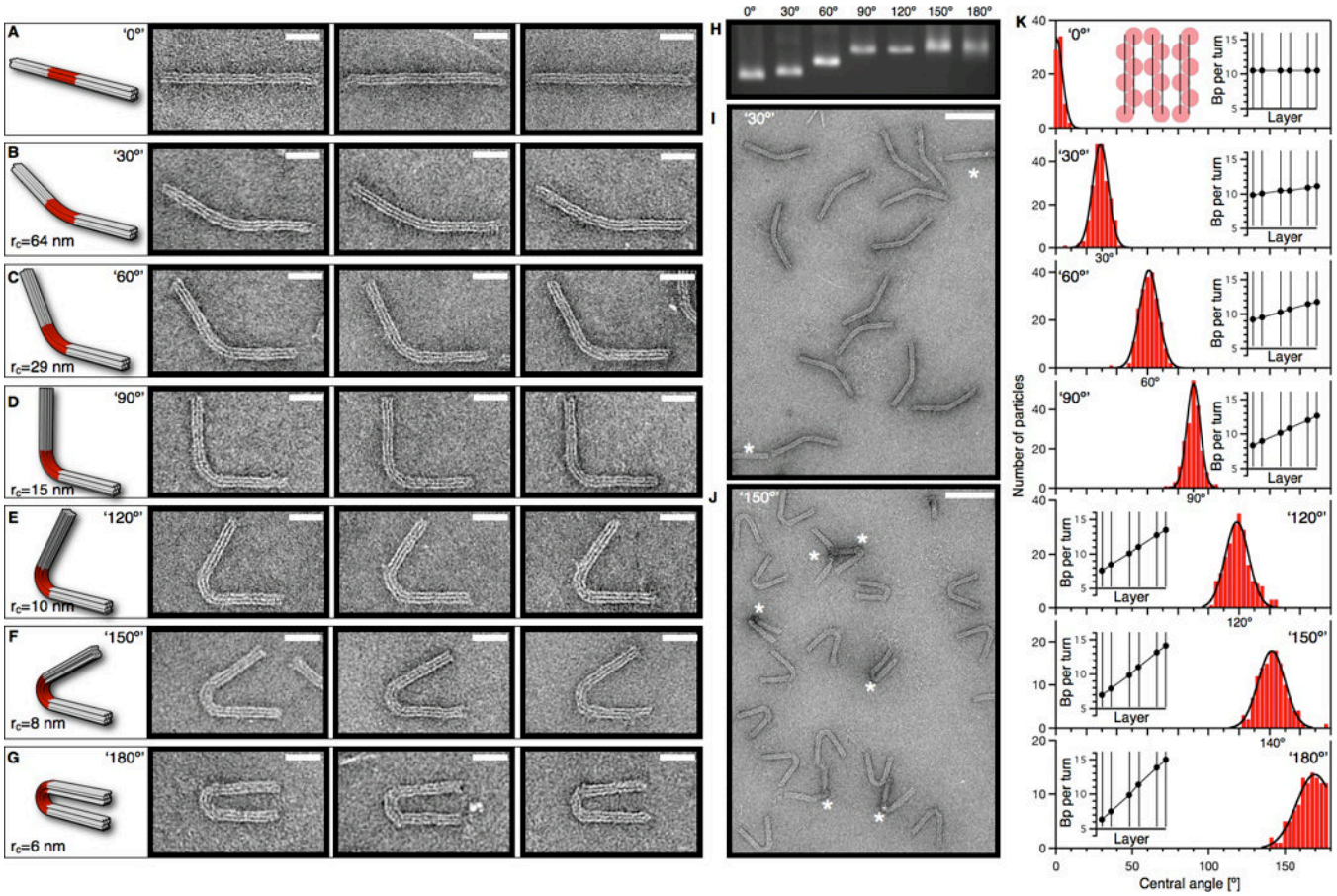

Figure 3.

Combining site-directed insertions and deletions induces globally bent shapes. **(A–G)** Models of seven 3 by 6-helix-bundle versions programmed to different degrees of bending and typical particles as observed by negative-stain TEM. Scale bars: 20 nm. **(H)** Ethidium-bromide-stained 2% agarose gel comparing migration of unpurified folding products of the seven differently bent bundles. **(I, J)** Low-magnification TEM micrographs of the bundle versions programmed to bend by 30° and 150°, respectively. Scale bars: 100 nm. **(K)** Histograms of bend angles as observed in individual particles for the seven different bundle versions. Average bend angles were determined to be 0°±(3° s.d.) (N=74); 30.7°±(5.4° s.d.) (N=212); 62.4°±(5.9° s.d.) (N=208); 91.3°±(5.2° s.d.) (N=206); 121°±(8.4° s.d.) (N=212); 143.4°±(9° s.d.) (N=131); 166° ±(9° s.d.) (N=106). Insets: Plot of average double-helical twist density through the cross section of the bent segment that results from the pattern of insertions and deletions installed to induce bending.

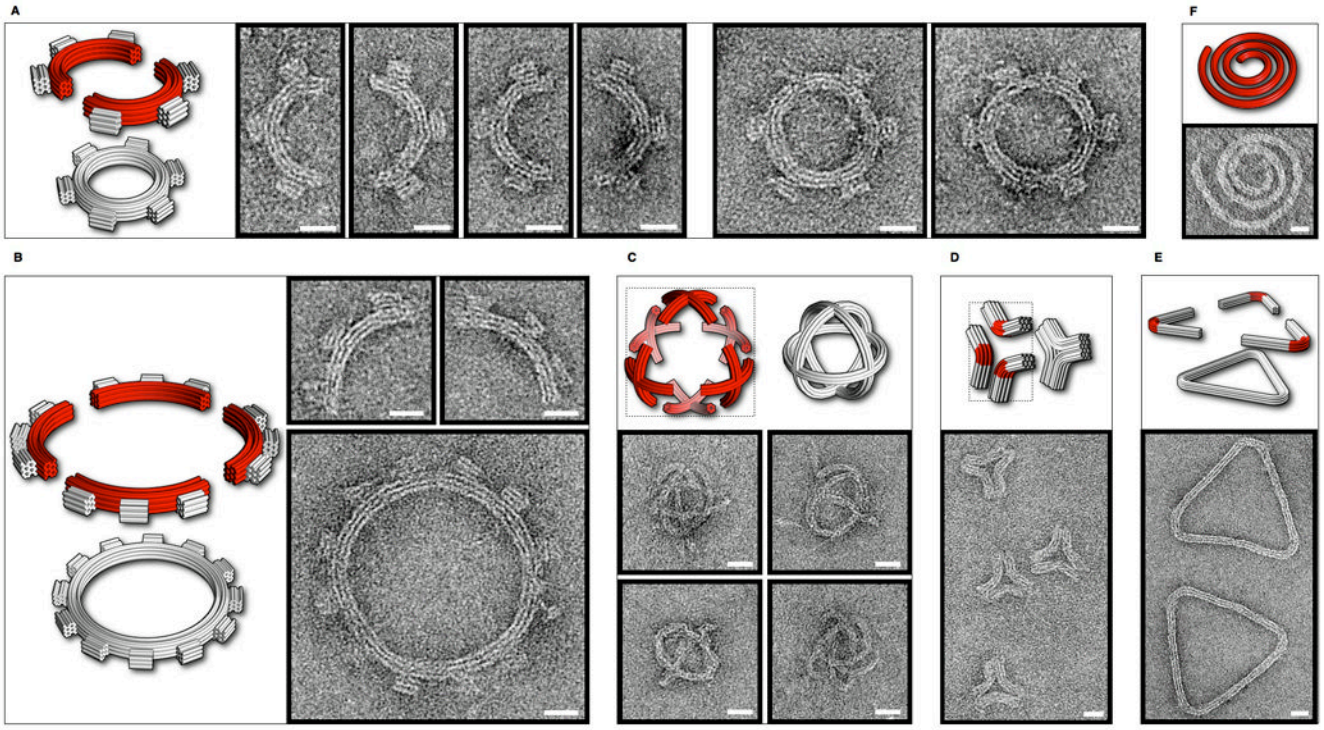

Figure 4.

Bending enables design of intricate nonlinear shapes. Scale bars: 20 nm. **(A)** Model of a 3 by 6-helix DNA-origami bundle designed to bend into a half-circle with a 25 nm radius that bears three non-bent teeth. Monomers were folded in separate chambers, purified, and mixed with connector staple strands to form six-toothed gears. Typical monomer and dimer particles visualized by negative-stain transmission electron microscopy (TEM). **(B)** 3 by 6-helix bundle as in (A), modified to bend into a quarter circle with a 50 nm radius. Hierarchical assembly of monomers yields 12-tooth gears. **(C)** A single scaffold strand designed to fold into a 50-nm-wide spherical wireframe capsule resembling a beach ball and four typical particles representing different projections of the beach ball. The design folds as six bent crosses (inset) connected on a single scaffold. **(D)** A concave triangle that is folded from a single scaffold strand. The design can be conceptualized as three 3 by 6 bundles with internal segments designed to bend by 60°. **(E)** A convex triangle assembled hierarchically from three 3 by 6 bundles designed with a 120° bend (Fig. 3E). **(F)** A six-helix bundle programmed with varying degrees of bending folds into a spiral-like object.